Magnetic field attenuation by thin superconducting lead films*†

H. R. Kerchner‡ and D. M. Ginsberg
Department of Physics and Materials Research Laboratory, University of Illinois, Urbana, Illinois 61801
(Received 28 May 1974)

Measurements have been made of the attenuation of an axial dc magnetic field by cylindrical thin films of superconducting lead. The normal-state resistance of each film was measured to determine the film thickness and the electron mean free path. The results have been used to derive the superconducting conductivity and the London-limit penetration depth $\lambda_L(T)$, and to infer the penetration depth $\lambda(T)$, which would be expected for pure bulk lead. Our experimental results for the temperature dependence of the superconducting conductivity and its value in the limit of zero temperature show unmistakable strong-coupling effects which agree well with our own theoretical calculations from previously obtained tunneling data and with published zero-temperature theoretical values. The analysis of the data indicates that $\lambda_L(0) = 315 \pm 7$ Å and the bulk zero-temperature penetration depth $\lambda(0)$ should be 453 ± 8 Å.

I. INTRODUCTION

One of the reasons for continuing interest in the superconducting properties of lead is the strong electron-phonon coupling which it exhibits. This strong coupling in lead and some of the other superconductors gives rise to important deviations from the BCS theory[1] in the density of states and other equilibrium and nonequilibrium properties.[2] As a result of a series of measurements of the electromagnetic response of lead at far-infrared frequencies, the importance of strong-coupling effects has become clear.[3,4] Two theoretical calculations[5,6] have explained in detail, at least at zero temperature, the influence of the strong electron-phonon coupling on these properties.

The far-infrared measurements and the theoretical calculations indicate that in the low-frequency limit the ratio of the superconducting to normal-state conductivity (at zero temperature) for lead is 20–26% lower than one would calculate from weak-coupling theory.[3,5,6] This particular strong-coupling effect has not previously been actually observed for any superconductor at a frequency lower than 3×10^{11} Hz. The absolute value of the penetration depth has not been measured with sufficient reproducibility to confirm or deny the existence of an important strong-coupling effect. Because of the absence of finite-temperature calculations relating to the electrodynamics of lead, adequate interpretation of measurements of the temperature dependence of the penetration depth has been impossible.[7]

We have measured the attenuation of a dc axial magnetic field by cylindrical thin films of superconducting lead. We have also measured the normal-state resistance of the same films at various temperatures. From these two sets of measurements the ratio of the conductivity in the superconducting state to that in the normal state and the London-limit penetration depth were determined. We have also calculated the same conductivity ratio for finite temperatures from tunneling data by using the strong-coupling theory, and our experimental results are compared with the theoretical results.

There have been a number of previous measurements of the penetration depth of lead, both its zero-temperature value[8–10] and its temperature dependence.[7,8,10–13] The results of these measurements range from 390 to 630 Å for the zero-temperature value.[9,10] One of the reasons for the discrepancies is that, because of the nonlocal nature of the relation between the current density and the vector potential, the results of different experiments are not directly comparable. Since the coherence length ξ_0 and the bulk penetration depth λ are of the same order of magnitude, neither the London limit ($\xi_0 \ll \lambda$) nor the Pippard limit ($\xi_0 \gg \lambda$) should be used for calculations; this makes penetration depth measurements difficult to interpret and compare. Even so, comparisons can be made, and the discrepancies among measurements of the penetration depth in lead are too large to be accounted for by nonlocal effects.

II. THEORY

A. Attenuation of an axial magnetic field by an infinitely long cylindrical superconducting thin film

In this section we relate our data to microscopic parameters of interest. We calculate the attenuation of an applied magnetic field H_0 by an infinitely long cylindrical superconducting film of thickness d. There is a uniform axial field H_i inside the cylinder and a uniform axial field H_0 outside. The difference in field strengths is

$$H_0 - H_i = \frac{4\pi}{c}\int_0^d J(x)\,dx\ , \tag{1}$$

where d is the film thickness and $J(x)$ is the current density in the film as a function of the dis-

tance x from the inner surface. If the vector potential were uniform over the film, the integral in Eq. (1) could be reduced to a conductance times the vector potential A. We could then write

$$H_0 - H_i = (4\pi i\omega/c^2)\,\sigma_s(\omega, T, d)\,A_\omega d\ , \tag{2}$$

where $\sigma_s(\omega, T, d)$ is the conductivity of the film at angular frequency ω and temperature T.

It remains to be shown that the vector potential is approximately uniform over the thickness of the film so we can use Eq. (2). The magnetic flux through a circular surface whose edge is at the inner surface of the film is $\pi a^2 H_i$, where a is the radius of the cylinder. We use the gauge $\vec{A} = \frac{1}{2}\vec{H}\times\vec{r}$, and put the point $\vec{r}=0$ on the cylinder's axis. Then the vector potential at the inner surface of the film is

$$A = \tfrac{1}{2}aH_i\ . \tag{3}$$

The flux passing through a surface with edges at the inner and outer surfaces of the film is clearly less than $2\pi adH_0$. Thus we can give upper and lower bounds to the vector potential inside the film,

$$\tfrac{1}{2}aH_i \le A < \tfrac{1}{2}aH_i[1 + (2d/a)(H_0/H_i)]\ . \tag{4}$$

For all our films, $2dH_0/aH_i < 0.04$. We therefore substitute the approximation (3) for the vector potential into Eq. (2) to obtain

$$r(T) - 1 = (2\pi i\omega ad/c^2)\,\sigma_s(\omega, T, d)\ , \tag{5}$$

where we define the attenuation ratio

$$r(T) = H_0/H_i\ . \tag{6}$$

The relation between current density and the electromagnetic field in a superconductor is commonly written in the form[14]

$$\vec{J}(\vec{r}, \omega) = \frac{N(0)e^2 v_F}{2\pi^2 c\hbar}\int \frac{\vec{R}[\vec{R}\cdot\vec{A}_\omega(\vec{r}')]}{R^4}\, I(\omega, R, T)\, d^3r'\ , \tag{7}$$

where $N(0)$ is the density of states at the Fermi surface, v_F is the Fermi velocity, $\vec{R} = \vec{r} - \vec{r}'$, and $\vec{A}_\omega(\vec{r}')$ is the vector potential in the London gauge at angular frequency ω and position $\vec{r}'$. [The kernel I in Eq. (7) differs from that in Ref. 15 by a factor of $\hbar$.] If we use Pippard's approximation[1,16]

$$I(0, R, T) = I(0, 0, T)e^{-R/\xi(l,T)}\ , \tag{8}$$

where

$$\xi(l, T) = \xi_0(T)l/[\xi_0(T) + l] \tag{9}$$

and[17,18]

$$\xi_0(T) = \int_0^\infty I(0, R, T)\, dR/I(0, 0, T)\ , \tag{10}$$

the zero-frequency limit of Eq. (7) becomes formally analogous to Chambers's expression for the current density in a normal metal.[19] We make use of this analogy to derive a simple expression relating $r(T)$ to the static local value $I(0, 0, T)$ of the kernel $I(\omega, R, T)$.

Fuchs[20] calculated the ratio of the normal-state conductivity $\sigma_n(d)$ of a thin film of thickness d to that σ_n of a bulk material of the same composition. He found that

$$\sigma_n(d)/\sigma_n = 1/F(d/l)\ , \tag{11}$$

where

$$1/F(x) = 1 - \frac{3}{8x} + \left[\frac{3}{8x} - \frac{5}{8} + \frac{1}{16}(x^2 - x)\right]e^{-x} + (\tfrac{3}{4}x)(1 - x^2/12)\int_x^\infty (e^{-t}/t)\,dt\ , \tag{12}$$

and l is the electron mean free path. Likewise, the superconducting conductivity of a thin film obeys the relation

$$\lim_{\omega\to 0}\left[\frac{\sigma_s(\omega, T, d)}{\sigma_s(\omega, T)}\right] = \frac{1}{F(d/\xi(l, T))}\ , \tag{13}$$

where the bulk superconducting conductivity $\sigma_s(\omega, T)$ should be calculated from Eq. (7) by using the same procedure one uses to find σ_n from Chambers's formula. To find $\sigma_s(\omega, T)$ we assume that $\vec{A}(\vec{r}')$ varies slowly enough so that we can take it out of the integral in Eq. (7) just as we would do to obtain the normal-state conductivity. Then it follows that

$$\lim_{\omega\to 0}\left[\frac{\omega\sigma_s(\omega, T)}{\sigma_n}\right] = \frac{-I(0, 0, T)}{i\pi\hbar}\,\frac{\xi(l, T)}{l}\ . \tag{14}$$

Combining Eqs. (5), (11), (13), and (14), we find

$$r(T) = 1 - 2a\gamma(T)I(0, 0, T)\sigma_n(d)\,d/\hbar c^2\ , \tag{15}$$

where

$$\gamma(T) = \frac{F(d/l)}{F(d/\xi(l, T))}\Big/\left(1 + \frac{l}{\xi_0(T)}\right)\ , \tag{16}$$

or in mks units,

$$r(T) = 1 - \mu_0 a\gamma(T)I(0, 0, T)/2\pi\hbar R_f\ , \tag{17}$$

where $R_f = 1/\sigma_n(d)d$ is the measured residual resistance which the film would have if it were square, and μ_0 is the permeability of free space. This is the desired relation between the microscopic parameters of interest and the field-attenuation ratio which we measure. In the limit $d/\xi(l, T) \ll 1$, Eq. (15) is identical to Peter's result.[21]

We calculate values of $I(0, 0, T)/\hbar$ from our experimental measurements. We can make a direct comparison between our experimental values for $I(0, 0, 0)/\hbar$ and the previously calculated values of that limit[5,6] by noting that those calculations assume that $l/\xi_0 \ll 1$. Under this assumption, Eq. (14) becomes

$$\lim_{\omega \to 0} \omega \sigma_s(\omega, T)/\sigma_n = -I(0, 0, T)/i\pi\hbar \ . \qquad (18)$$

In order to use Eq. (17) to interpret measurements of the field attenuation we need to know the values of d, l, and $\xi_0(T)$. Our theoretical calculations of $\xi_0(T)$ for lead have been reported previously.[15] We determined d and l by measuring the normal-state resistance of the film at room temperature and just above the superconducting transition temperature. The method has been discussed previously[22]; it makes use of Matthiessen's rule and Fuchs's expression for the resistivity of a thin film.[20] In addition to the two measurements of the film resistance, we required values of the resistivity of pure bulk lead at the same two temperatures and a value for the temperature-independent parameter ρl, where ρ is the resistivity. We obtained the resistivity normalized to the 0 °C value by interpolating data found in Ref. 23. For the resistivity at 0 °C we used the average of several experimental values,[23] which is 1.95×10^{-7} Ωm. The parameter ρl is related to the free area of the Fermi surface S. Measurements of S in lead have been reviewed by Gasparovic and McLean[7] and by Grimvall.[24] The two most recent and most reliable determinations of S give $S/S_0 = 0.70$, where S_0 is the value of S according to the free-electron theory. This value for S/S_0 corresponds to reconstructions of the Fermi surface from de Haas-van Alphen measurements[25] and from observations of Kohn anomalies in phonon-dispersion relations obtained by neutron diffraction.[26] Previously, values of 0.46 and 0.55 were obtained from S/S_0 from anomalous skin-effect measurements.[27,28] Assuming that $S/S_0 = 0.70$, we find $\rho l = 0.70\times10^{-15}$ Ωm^2. In order to take account of the possibility that future measurements will show that S/S_0 is smaller than 0.70, we have graphed our results as functions of the value assumed for ρl in our determinations of d and l.

B. Zero temperature value and temperature dependence of the kernel $I(0,0,T)$

In carrying out our previously reported calculations of the electromagnetic coherence length in lead,[15] we calculated the kernel $I(0, 0, T)$ by using the strong-coupling theory of Nam[29] and two finite-temperature models for the gap parameter in lead.[30,31] In Fig. 1 we compare our values for $I(0, 0, T)$ with the equivalent results calculated from weak-coupling theory. (Also shown is a curve representing our experimental results; these were derived from data on five different samples by a method described in Sec. VI.) Several models are listed in Fig. 1. Model 1 is Swihart's calculation of the frequency- and temperature-dependent complex gap parameter $\Delta(\omega, T)$ from a two-Lorentzian approximation to the phonon density of states.[30] Model 2 is Vashishta and Carbotte's calculation of $\Delta(\omega, T)$ from a tunneling-derived phonon density of states.[31] The result for model 3 is derived from Shaw and Swihart's calculation[6] for lead of $\sigma_1(\omega)$, the real part of the superconducting conductivity normalized to the normal-state value (in the limit of short electron mean free path). They used a tunneling-derived phonon density of states. Model 4 is Nam's calculation of $\sigma_2(\omega)$, the imaginary part of the superconducting conductivity normalized to the normal-state value.[5] He used the gap function of Schrieffer, Scalapino, and Wilkins, which they derived from a two-Lorentzian approximation to the phonon density of states.[32] According to weak-coupling theory,[14] the kernel is given by

$$I(0, 0, T) = -\pi^2\Delta_0(0)J(0, T)\Lambda_0/\Lambda_T$$
$$= -\pi^2\Delta_0(T)\tanh\left(\frac{\alpha}{4t}\frac{\Delta_0(T)}{\Delta_0(0)}\right) , \qquad (19)$$

where $\alpha = 2\Delta_0(0)/kT_0$, $\Delta_0(T)$ is the BCS gap parameter, $t = T/T_c$ is the reduced temperature, and Λ_T and $J(0, T)$ are BCS functions.[1] In the BCS weak-coupling theory, the value of α is 3.53. However, the curve representing weak-coupling theory in Fig. 1 is scaled by setting α equal to 4.3, the measured value for lead.[33] The zero-temperature gap parameter assumed is the measured value[33] of 1.34 meV.

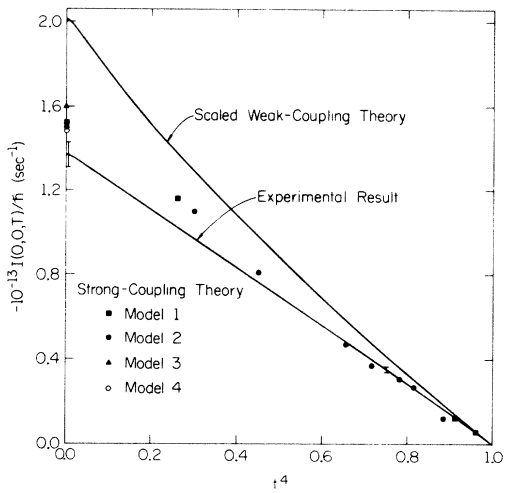

FIG. 1. Static local value of the kernel, $I(0, 0, T)$, plotted as a function of t^4, where $t = T/T_c$. The experimental curve is derived from the expression which we fitted to the data, Eq. (19), using the best values of $I(0, 0, 0)$ and α obtained from data on five different samples. The error bars represent the standard deviation of the best experimental value of $I(0, 0, T)$ for T near zero and near T_c.

III. EXPERIMENTAL PROCEDURE

A. Sample preparation

Each of our samples was deposited in high vacuum ($\sim 5\times10^{-6}$ Torr) onto the outside of a liquid-nitrogen-cooled rotating cylindrical Pyrex tube by evaporating 99.999% pure lead from a hot molybdenum boat in about 20 sec. The procedure was similar to that used previously to prepare indium samples.[34]

We were not able to join our lead films to silver electrical contacts as described in Ref. 34 because of a reaction between the silver and the lead. Therefore, we used thicker (5000 Å) contacts composed of lead. We attached copper wires to these contacts with indium solder after the sample was mounted in the cryostat.

B. Superconducting magnetometer

The magnetometer was based on a superconducting quantum interference device (SQUID) originally devised by Silver and Zimmerman.[35] Our SQUID was furnished by the S.H.E. Corp. The SQUID was coupled to the magnetic field to be measured by means of a superconducting flux transformer. We used the SQUID in conjunction with a 19-MHz oscillator, a tuned amplifier and detector, and a lock-in amplifier that operated at 1 kHz. The electronics constituted a linear-feedback network. The feedback produced a null in the current in the flux transformer.[34] Thus, there was no distortion of the field by persistent currents in the transformer circuit.

We cycled the applied field H_0 many times and accumulated data in a multichannel signal averager. Since this device generated rf currents which could disrupt the operation of the magnetometer, it was necessary to place the signal averager inside a copper screen box and connect the inputs through rf filters.[36]

C. Cryostat and field coils

Except for the superconducting magnetometer, the cryostat and magnetic field coils were identical to the equipment described previously.[34] We give only a brief description here.

The cryostat was designed to cool the sample and the superconducting parts of the magnetometer separately. The magnetometer was enclosed in a probe that extended from the top of the cryostat axially through the center of the sample. Two chambers, which were magnetically shielded by superconducting shielding, contained the SQUID and the coil that coupled feedback flux to the flux transformer. These chambers were located 0.5 m above the sample so that the field distortion they created would be negligible near the sample. The portion of the flux transformer connecting the field-sensing coil with the parts inside the shielded chambers also was shielded by a Sn-Pb alloy superconducting tube. This tube extended from inside the lower shielded chamber to below the lower end of the sample. It was located on the sample axis so that the cylindrical symmetry would be preserved. The superconducting wires emerged from inside the tube through a small hole in one side to form the field-sensing coil. The portion of the magnetometer probe containing the SQUID and the flux transformer was kept at 4.2 K by the outer bath of liquid helium.

The sample chamber was thermally isolated from the outer helium bath by a vacuum space. It was cooled below 4.2 K by an inner tank of liquid helium. To reach temperatures above 4.2 K we evacuated the inner tank except for some helium exchange gas, and we heated the sample chamber electrically. The exchange gas provided a weak thermal link between the sample chamber and the outer bath. The sample chamber itself contained helium exchange gas to insure that all parts of the sample were in thermal equilibrium. We measured the temperature by using a calibrated germanium resistance thermometer. For fine temperature control we used an electronic temperature regulator to drive the heater. The regulator was activated by a carbon resistance thermometer which sensed temperature changes.

Magnetic fields were generated by three sets of coils. The main coils produced the uniform axial field. Saddle-shaped coils[37] canceled the horizontal component of the earth's field. A pair of end coils, which were situated just beyond the ends of the sample, compensated for end effects. In order to adjust the current in the end coils precisely, we made this adjustment while measuring the attenuated field change near the end of the sample. In this way we could match the actual measured field as a function of position along the sample axis to the field calculated in designing the end coils.[36]

By monitoring the resistance of the sample we aligned the axial field with the sample and canceled the horizontal component of the earth's field as had been done previously for indium samples.[34] Comparison of measurements taken with the saddle-shaped coils in use with those taken while they were disconnected showed that the presence of the earth's field had little effect on the measurements. On the other hand, the uncertainty of 1° in the alignment of the applied axial field was responsible for a large portion of the uncertainty in our results.

We found it necessary to shield the magnetometer from the 60-Hz magnetic fields generated by vacuum pumps and transformers. For this purpose we used two copper cylinders, one in the liquid-nitrogen bath and one in the liquid-helium bath. Together, these two shields attenuated the 60-Hz field

by a factor of 1000. Each shield had a time constant $L/R = 0.08$ sec.

D. Acquisition of magnetic data

During the measurement of the magnetic field attenuation ratio, the main-field coils and end solenoids were driven by a function generator. The applied magnetic field signal was a symmetrical triangle wave with a period of about 10 sec. Its amplitude varied from 2 to 100 mG, depending on the maximum field sweep we could use before hysteresis became observable.[34] Using the signal averager, we typically averaged 64 complete waveforms of the feedback current, which was proportional to the change in field strength. Our measure of the field change was the average absolute value of the slope on the two sides of this averaged complete waveform.

Immediately after completing each magnetic field measurement, we measured the slope of the voltage output of the function generator. We normalized the magnetic field measurement by dividing it by this slope to eliminate long-term drifts in the voltage output and period of the function generator and in the resistance of the rf filters.

To calibrate the magnetometer, we determined the field change at the center of the sample as described above while the sample was warmed above its transition temperature. Our resulting data were measurements of the ratio $r(T) = \Delta H_0/\Delta H_i$ of the applied field change to the attenuated field change.

IV. RESULTS

A. Film resistance and thickness

In order to calculate $\gamma(T)$, defined in Eq. (16), it was necessary to determine the thickness d and the electron mean free path l for each sample. We calculated these quantities from measured values of the film resistance at room temperature and at a temperature just above the resistive transition.[22]

In Table I we show for each sample the values of film thickness d and electron mean free path l corresponding to the lowest and highest values of ρl that we assumed for our analysis of the field-attenuation measurements. The film thickness depends only weakly on ρl, but the mean free path varies almost exponentially[36] with ρl.

We measured the film resistance at several temperatures between the transition temperature and room temperature. These data[36] for samples 2, 3, and 4 were consistent with the theoretical temperature dependence[22] for values of ρl between 0.7 and 1.1×10^{-15} Ωm^2. The data for samples 1 and 5 were less scattered and indicated that ρl was close to 0.7×10^{-15} Ωm^2 for sample 1 and to 1.1×10^{-15} Ωm^2 for sample 5.[36] It is likely that the theoretical approximation of isotropic scattering fails at intermediate temperatures, where scattering by low-energy phonons dominates the behavior of the film resistance. This may account for the apparent difference between the values of ρl for samples 1 and 5.

Also listed in Table I are values for T_c and δT_c. The transition temperature T_c is here defined as the temperature at which the film's resistance was one-half of its normal-state value. The transition width δT_c is defined as the temperature interval in which the film's resistance increased from $\frac{1}{4}$ to $\frac{3}{4}$ of its normal-state value.

B. Attenuation data—comparison with theory

1. Introduction

The principal data of this experiment are shown in Fig. 2; they are the measurements of the ratio $r(T)$ of the applied field change to the attenuated field change, $\Delta H_0/\Delta H_i$, as a function of temperature. According to Eq. (17), that ratio should depend on temperature approximately in proportion to $I(0, 0, T)$, because $\gamma(T)$ is only a weak function of temperature. The data of Fig. 2 do in fact look very similar to the plots of $-I(0, 0, T)$ in Fig. 1.

We invert Eq. (17) to obtain $I(0, 0, T)$ from the experimental data for comparison with theoretical values. To calculate the factors preceding $I(0, 0, T)$ in Eq. (17), we use our knowledge of the film thickness and the electron mean free path and the theoretical result[15] for the coherence length. Since we need to know $I(0, 0, T)$ in order to calculate the coherence length, this procedure for interpreting our data appears to be a circular process. Actually, the explicit proportionality between $\Delta H_0/\Delta H_i$ and $I(0, 0, T)$ dominates the implicit dependence of $I(0, 0, T)$ on the other factors in Eq. (17). There are many uncertainties which are of about the same importance as the one due to the difference between measured values of $I(0, 0, T)$ and the value assumed in the calculation of the coherence length.

2. Fitting procedures

In order to obtain numerical information from our data that would be both simple to handle and complete, we fitted a simple theoretical formula to our data by a least-squares technique. We rewrote Eq. (17) in terms of the reduced kernel

TABLE I. Transition temperature, transition width, film thickness, and electron mean free path.

Sample	T_c (K)	δT_c (K)	$\rho l = 0.7\times10^{-15}$ Ωm^2 d (Å)	l (Å)	$\rho l = 1.1\times10^{-15}$ Ωm^2 d (Å)	l (Å)
1	7.157	0.007	85	1936	91	8991
2	7.146	0.018	105	510	109	1526
3	7.170	0.019	139	447	142	1245
4	7.185	0.003	145	637	149	1968
5	7.176	0.009	148	621	152	1892

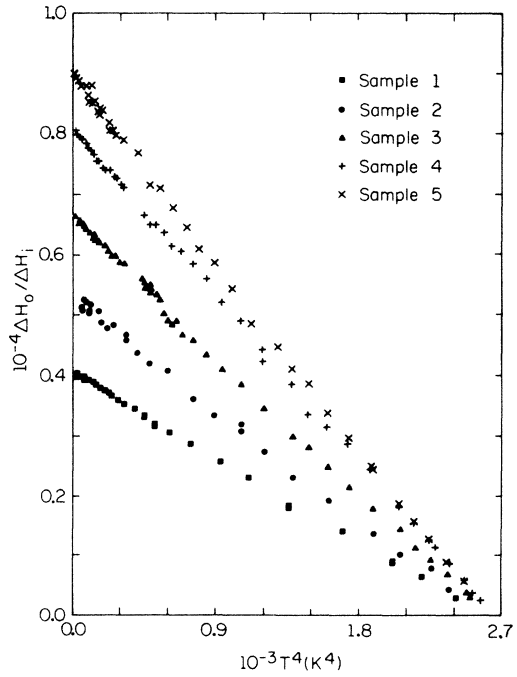

FIG. 2. Dependence of the magnetic field attenuation data on T^4.

$I(0,0,T)/I(0,0,0)$ and the extrapolation of the data to zero temperature. For the reduced kernel we used the expression given by Eq. (19). Then the reformulation of Eq. (17) is

$$r(T) = 1 + [r(0) - 1]\frac{\gamma(T)\Delta_0(T)}{\gamma(0)\Delta_0(0)}\tanh\left(\frac{\alpha}{4t}\frac{\Delta_0(T)}{\Delta_0(0)}\right). \quad (20)$$

We allowed $r(0)$, α, and T_c to vary and found the values of these parameters that minimized the sum of the squares of the fractional deviations of the measured values of $\Delta H_i/\Delta H_0$ from the values of $1/r(T)$ given by Eq. (20). Since our function $1/r(T)$ is nonlinear in the three parameters, we found the best values for them by using an iterative numerical technique, the Newton-Raphson method.[38]

We chose the expression in Eq. (19) to fit our data for several reasons. First, it is simpler to evaluate by computer than some complicated parametrized version of an expression from strong-coupling theory. Second, in contrast to some arbitrary function of T, it is derived from an energy-gap theory of superconductivity, and therefore can be expected to show the correct qualitative temperature dependence. Third, it was used successfully to describe a previous measurement of the temperature dependence of the magnetic field attenuation by cylindrical thin films of lead.[12,13] However, it should be emphasized that the theoretical results presented in Fig. 1 indicate that the values of both $I(0,0,0)$ and α which are derived from our data can be expected to differ substantially from the values of the corresponding BCS expressions, $-\pi^2\Delta_0(0)$ and $2\Delta_0(0)/kT_c$, respectively.

To calculate $\gamma(T)$, we needed to know $\xi_0(T)$; for this we used a function from weak-coupling theory to approximate the temperature dependence of the coherence length:

$$\xi_0(T) = \xi_0(0)/J(0,T) . \quad (21)$$

This temperature dependence is the curve labeled $2\Delta(0)/kT_c = 3.528$ in Fig. 4 of Ref. 18. It describes quite well the temperature dependence of the coherence length in lead, which we reported previously.[15] We assumed that $\xi_0(0) = 1290$ Å, determined as before.[15] We needed Λ_T/Λ_0 to evaluate[18] the function $J(0,T)$, since

$$J(0,T) = \frac{\Lambda_T\Delta_0(T)}{\Lambda_0\Delta_0(0)}\tanh\left(\frac{0.882}{t}\frac{\Delta_0(T)}{\Delta_0(0)}\right). \quad (22)$$

To evaluate the BCS functions $\Delta_0(T)/\Delta_0(0)$ and Λ_T/Λ_0 we interpolated Mühlschlegel's tables of these functions.[39] Near the critical temperature such an interpolation would not be accurate; therefore, when $T > 0.98\ T_c$, we used a limiting expression[39] for $\Delta_0(T)/\Delta_0(0)$ and approximated $1/J(0,T)$ by the linear function of T that passed through the points $1/J(0, 0.98\ T_c)$ and $1/J(0,T_c)$.

The curve-fitting procedure was carried out five

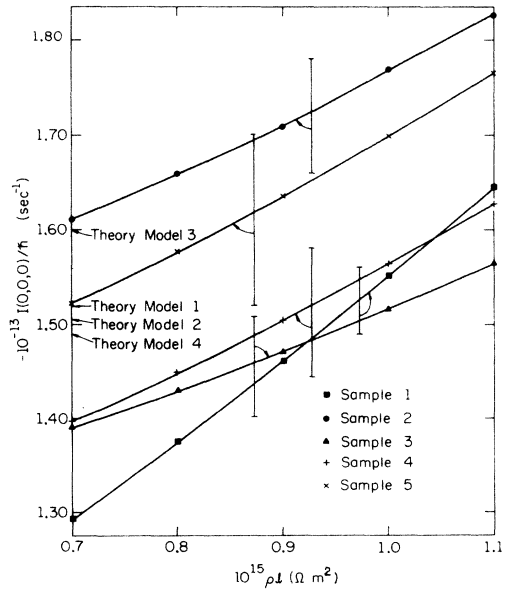

FIG. 3. Dependence of the experimental results for the zero-temperature kernel $I(0,0,0)$ on the value assumed for ρl. Indicated on the vertical axis are the theoretical values discussed in Sec. II B.

times for each sample, once for each of five values of ρl between 0.7 and 1.1×10^{-15} Ωm^2. If Eq. (2) can be made to fit the data accurately for all values of ρl, then the best values of T_c and $\gamma(0)$ should not depend strongly on ρl. This was indeed the case; the best values of T_c varied by less than 0.001 K, and the best values of $\gamma(0)$ varied by less than 1% as ρl was varied from 0.7 to 1.1×10^{-15} Ωm^2.

3. *Value of the kernel at absolute zero*

From the best value of $\gamma(0)$ and a calculation of $\gamma(0)$ we can immediately obtain the zero-temperature, zero-frequency kernel $I(0,0,0)$ from Eq. (17). The result for each sample is shown as a function of ρl in Fig. 3. Also indicated on the vertical axis are the theoretical results, which were discussed in Sec. II B. This experiment confirms the theoretical prediction[5,6] of a low zero-frequency kernel and conductivity, about 20 to 26% lower than one would obtain from the weak-coupling theory. [Note that the weak-coupling value is $I(0,0,0)/\hbar = 2.01\times10^{13}$ sec^{-1}.]

Our experimental results for $I(0,0,0)$ depend on the value assumed for the renormalized[40] Fermi velocity v_F^* through the dependence[15] of $\xi_0(0)$ on v_F^*. However, the dependence is rather weak,

$$\frac{v_F^*}{I(0,0,0)}\frac{\partial I(0,0,0)}{\partial v_F^*} = -0.28\ . \tag{23}$$

We now consider how our conclusions would change if we assumed that the electrons were specularly reflected from the surfaces of the film rather than diffusely, as we believe to be the case. In place of Eq. (12) we would have $F(x)=1$. Using this value in Eq. (16) and in our derivation of d and l from the film resistance, we find that $I(0,0,0)$ would be 2% lower than the curves of Fig. 1 at $\rho l = 0.7\times10^{-15}$ Ωm^2 and 8% lower at 1.1×10^{-15} Ωm^2, except for sample 1. For that sample, the assumption of specular reflection would imply that $I(0,0,0)$ would be 10% and 23% below the diffuse scattering result for $\rho l = 0.7$ and 1.1×10^{-15} Ωm^2, respectively. Thus. assuming specular reflection would make the results for sample 1 very different from the results for the other samples.

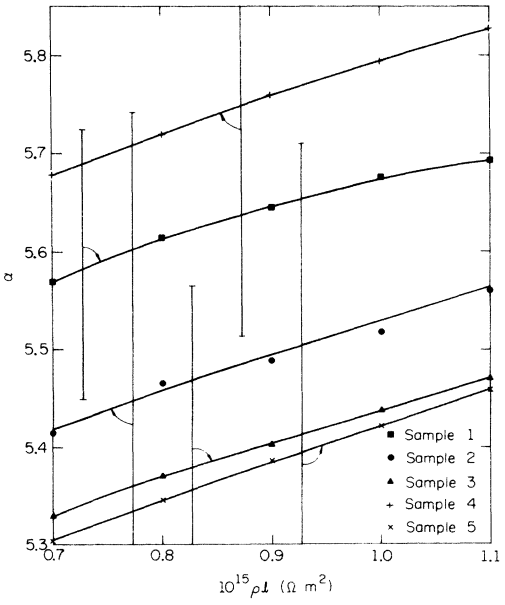

FIG. 4. Dependence of the experimental results for α on the value assumed for ρl.

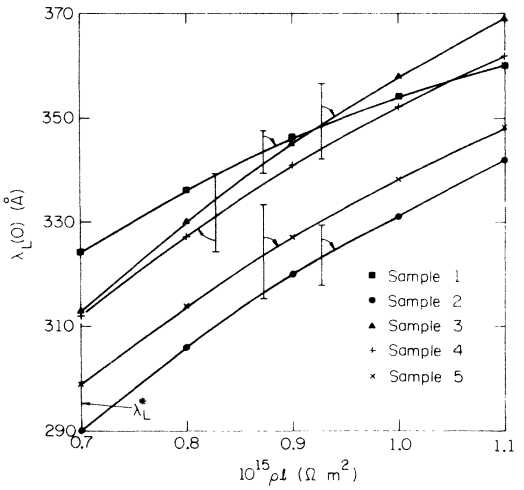

FIG. 5. Dependence on the value assumed for ρl of the zero-temperature London-limit penetration depth calculated from our experimental results. Indicated on the vertical axis is the renormalized London penetration depth obtained from the low-temperature electron specific heat and the free area of the Fermi surface.

4. *Temperature dependence of the kernel*

We found that Eq. (20) describes the temperature dependence of the data quite well, for any of the values assumed for ρl. The root-mean-square percent deviation of the data from the best-fit function is between 1% and 2% for all samples except sample 2. The data for that sample are scattered somewhat more and the rms deviation is 4% because of an experimental problem.[36]

The temperature dependence of $I(0,0,T)/I(0,0,0)$ is determined according to Eq. (19) by the parameter α. The values of α obtained from our least-squares curve fitting are shown in Fig. 4. We see that α does not depend as strongly on the value assumed for ρl as does $I(0,0,0)$. Also, the variation of α with the value taken for v_F^* is small,

$$\frac{v_F^*}{\alpha}\frac{\partial\alpha}{\partial v_F^*} = -0.05\ . \tag{24}$$

5. London-limit penetration depth at absolute zero

We have derived the London-limit penetration depth at zero temperature from our measurements of $I(0,0,0)$ by using the relation[15]

$$\lambda_L^2(T) = [K(0,0,T)]^{-1/2}$$

$$= [-I(0,0,T)\xi_0(T)/\pi\hbar\lambda_L^2 v_F]^{-1/2} . \qquad (25)$$

For $\xi_0(0)$ we use our theoretical value.[15] To evaluate the quantity $\lambda_L^2 v_F$ we note that, like ρl, it depends only on the Fermi-surface area S, so we assume that $\lambda_L^2 v_F$ varies in proportion to ρl. In Fig. 5 we have graphed $\lambda_L(0)$ as a function of ρl. Also shown there is the value of the (renormalized[15]) London penetration depth λ_L^* which we calculated by using experimental values for the density of states at the Fermi surface[41,42] and the Fermi velocity.[15]

C. Uncertainties

We estimated the statistical uncertainty in each of the three parameters $r(0)$, α, and T_c by calculating the standard deviation of each parameter.[43] (See Table II.)

We estimated the uncertainty in our results due to systematic errors by measuring the field attenuation under deliberately nonideal conditions and comparing the results with our "ideal" data. We tilted the main-field coils by 1°, we altered the current in the end coils by 2%, and we introduced a static transverse field by turning off the saddle-shaped coils. We also turned off the end coils completely while repeating some of the measurements. The data taken under nonideal conditions led us to identify just two important sources of systematic error, possible misalignment of the main-field coils and possible asymmetries in the physical dimensions of the end coils.[36]

The systematic errors mentioned above and the additional systematic error which is introduced by approximating the vector potential by a constant in deriving Eq. (17) contribute to the uncertainty in our results for $I(0,0,T)$ in the same way; in each case, there is a constant additive contribution to $1/r(T) = \Delta H_i/\Delta H_0$. To determine the influence of such an error on our results, we altered our data by adding a constant to each value of $\Delta H_i/\Delta H_0$ and found new values for $I(0,0,0)$ and α for each sample. (We assumed $\rho l = 0.7\times10^{-15}$ Ωm^2.)

TABLE II. Percent standard deviation of the three parameters, from scatter only, not including possible systematic errors.

Sample	$r(0)$	α	T_c
1	0.36	0.87	0.014
2	1.47	3.81	0.071
3	0.32	0.78	0.010
4	0.54	1.05	0.008
5	0.26	0.61	0.011

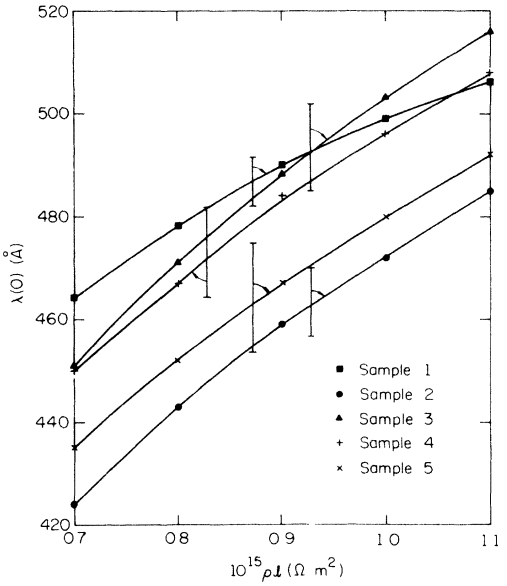

FIG. 6. Dependence on the value assumed for ρl of the zero-temperature bulk penetration depth calculated from our experimental results.

To calculate the probable accuracy of the results for each sample, we calculated the square root of the sum of the squares of the systematic and statistical uncertainties. (The fractional uncertainties were not sensitive to ρl.) We have indicated the results of these calculations in the error bars in Figs. 3 and 4. The error bars in Figs. 5–7 were calculated by finding the propagation of error in $I(0,0,0)$ and α to $\lambda_L(0)$, $\lambda(0)$, and $d\lambda/dy$. The fact that the error bars in Figs. 3 and 5–7 do not quite overlap is presumably due to variation in film structure from sample to sample.

V. COMPARISON WITH PREVIOUS PENETRATION DEPTH MEASUREMENTS

A. Temperature dependence of the kernel

In the Introduction we mentioned other types of experiments that qualify as penetration depth measurements. It is of interest to compare our results with them. Except for measurements of the field attenuation by cylindrical thin films, it is not possible to make a direct comparison of our results with those obtained by other means. For other types of experiments we use our results, together with some additional assumptions, to calculate the result one expects from each type of experiment.

The one experiment of the same type as ours was that of Erlbach, Garwin, and Sarachik.[13] They measured $r(T)/r(0)$ as a function of tempera-

ture by an rf technique and fitted their results to an expression from weak-coupling theory which is comparable to our Eq. (20). They took measurements only below 4.2 K, and assumed their films had transition temperatures equal to the transition temperature of bulk lead, $T_c = 7.22$ K. Their result (see Fig. 8 of Ref. 13), $\alpha = 5.4$, compares well with ours. Most of our values for α are slightly higher because we took into account the temperature dependence of the factor $\gamma(T)/\gamma(0)$. They did not measure the electron mean free path or calculate $\gamma(T)$. (They also did not avoid rf magnetic fields perpendicular to the sample surface, which may have driven parts of their samples normal.)

B. Penetration depth at absolute zero

In order to check the consistency of our measurements and theoretical calculations with other types of penetration depth measurements, we calculated the bulk penetration depth at zero temperature $\lambda(0)$. To find $\lambda(0)$ we used the graph of λ/λ_L vs ξ_0/λ_L in Fig. 7 of Ref. 1. For λ_L we use the values of $\lambda_L(0)$ presented in Fig. 5, and for ξ_0 we use our value calculated from strong-coupling theory.[15] The results of this calculation are presented in Fig. 6. [These values are derived by assuming diffuse scattering at the surface of our samples and at the surface of the hypothetical bulk sample. If we instead assumed specular reflection at the surface of the bulk sample (but still assume diffuse surface scattering for our films), the values of $\lambda(0)$ would all be 15% smaller than the values shown in Fig. 6.] Simon[8] measured the surface impedance of a bulk sample of lead at 9100 MHz and found $\lambda(0) = 540$ Å.

In calculating $\lambda(0)$ in this way, we have assumed that the spatial dependence of the kernel $I(0, R, T)$ is the same for lead as for a BCS superconductor (with our strong-coupling value for the coherence length). The strong-coupling numerical calculation of $\lambda(0)$ by Swihart and Shaw[44] supports our assumption. They find $\lambda(0)/\lambda_L(0) = 1.51$ and 1.29 in the diffuse scattering and specular reflection cases, respectively. Using their value for $\lambda_L(0)$ and the value for $\xi_0(0)$ that we obtain from their calculations,[15] we find $\lambda(0)/\lambda_L(0) = 1.54$ and 1.31 from Fig. 7 of Ref. 1. The discrepancy of 2% is about the size of the uncertainty that one would expect of the numerical methods of BCS.[45]

C. Temperature dependence of the penetration depth near the critical temperature

Very near T_c, $\lambda(T) \gg \xi_0(T)$; therefore $\lambda(T) = \lambda_L(T)$. Using Eqs. (25) and (19) we find

$$\frac{\lambda_L(T)}{\lambda_L(0)} = \left(\frac{\xi_0(0) I(0,0,0)}{\xi_0(T) I(0,0,T)}\right)^{1/2}$$

$$= \left[\frac{\xi_0(T)\Delta_0(T)}{\xi_0(0)\Delta_0(0)} \tanh\left(\frac{\alpha}{4t}\frac{\Delta_0(T)}{\Delta_0(0)}\right)\right]^{-1/2} . \quad (26)$$

Substituting $\Delta_0(T) = 0.868\,\Delta_0(0)(1 - t^4)^{1/2}$ (the weak-coupling expression,[39] which is consistent with tunneling measurements[46] and theory[31]), putting $T = T_c$, and using the small argument approximation to tanh, we find

$$\lim_{T \to T_c} \frac{d\lambda_L}{dy} = \lambda_L(0)/0.434 \left(\frac{\alpha \xi_0(T_c)}{\xi_0(0)}\right)^{1/2} , \quad (27)$$

where $y = (1 - t^4)^{-1/2}$. We assume that[15] $\xi_0(T_c)/\xi_0(0) = 0.75$ and average our experimental results (with $\rho l = 0.7 \times 10^{-15}$ Ωm^2). The average values are $\lambda_L(0) = 315$ Å and $\alpha = 5.51$. This gives $\lim_{T \to T_c} (d\lambda_L/dy) = 357$ Å.

Gasparovic and McLean measured the average value of $d\lambda/dy$ between $y = 2.75$ and 6.00 ($t = 0.965$ and 0.993).[7] Even at the higher temperature there is a substantial nonlocal correction to the penetration depth (i.e., $d\lambda_L/dy \neq d\lambda/dy$). Therefore, we calculated the penetration depth for $t = 0.965$ and $t = 0.993$ and subtracted the two values to obtain the average $d\lambda/dy$ in the range where it was measured. For $\lambda_L(T)$ we used the approximate relation

$$\lambda_L(T) = y \lim_{T \to T_c} \frac{d\lambda_L}{dy} . \quad (28)$$

Otherwise, the calculation proceeded just as for zero temperature. The results for each of our samples are compared with the result of Gasparovic and McLean in Fig. 7.

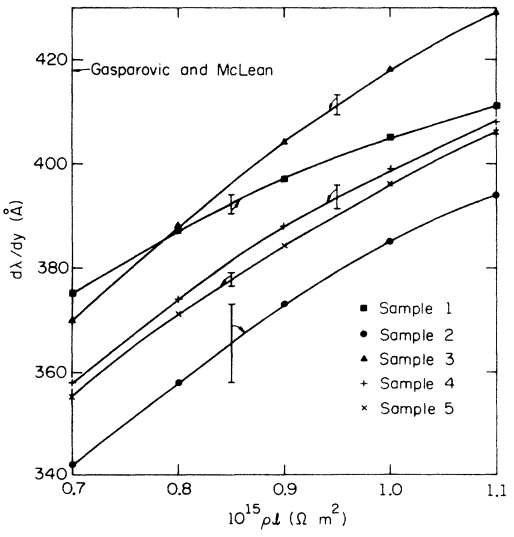

FIG. 7. Dependence on the value assumed for ρl of the average value of $d\lambda/dy$ between $y = 2.75$ and $y = 6.00$ calculated from our experimental results. Indicated on the vertical axis is the experimental result reported in Ref. 7.

They noted that their experimental results indicated that $d\lambda/dy$ increases slightly at lower temperatures. Our calculations of $\lambda(T)$ show the same qualitative behavior. However, Fig. 7 shows that there is a clear discrepancy between our results and theirs. Our curves come close to their value only for the higher values of ρl. These higher values are inconsistent with the more recent studies of the Fermi surface of lead, as we noted above.

D. Comparison with measurements of the magnetization of thin films

The results of experimental measurements of the magnetization of small superconducting specimens are usually expressed in terms of an effective penetration depth. This effective penetration depth is derived from the experimental data by assuming a local relation between the current density and the vector potential, a relation of the form of London's equation. Calculations have been carried out that relate the effective penetration depth measured in an experiment of this type to that for bulk material. The handiest result of these calculations is the formulation of Thompson and Baratoff.[47,48] We use Fig. 4 of Ref. 48 in the following.

Lock measured the magnetization of many planar films of about 2000-Å thickness.[9] He found an effective penetration depth at absolute zero of 390 ±30 Å. He did not report the electron mean free path for his samples. If we assume the values d = 2000 Å, $\xi(l, T) = \xi_0(0) = 1290$ Å, $\lambda_L(0) = 315$ Å, and diffuse surface scattering, we find $\lambda_d(0) = 445$ Å. Taking into account a finite mean free path would make this result larger.

Peabody and Meservey used a quantum interferometry method to measure the magnetization of just two films.[10] For their 1630-Å film, they found an effective penetration depth of 630 ± 50 Å. They give the room-temperature resistivity and the room-temperature to low-temperature resistance ratio of their film. From these numbers we obtain $l = 5000$ Å. Then our estimate of $\lambda_d(0)$ for their film is $\lambda_d(0) = 500$ Å.

VI. SUMMARY

We have measured the attenuation of a uniform axial magnetic field by cylindrical thin lead films. We determined the film thickness and electron mean free path from normal-state measurements. Knowledge of those parameters, along with our calculated value of the electromagnetic coherence length, allowed us to find the electromagnetic response kernel $I(0, 0, T)$ from our attenuation measurements.

Our results show that $I(0, 0, T)$ can be approximated quite well by the expression given in Eq. (19) with $\alpha = 5.5$. This is in marked contrast to the result of scaled weak-coupling theory, which requires that $\alpha = 4.3$ for lead. Furthermore, our experimental result for $-I(0, 0, 0)$ is about 30% smaller than the value according to scaled weak-coupling theory, $\pi^2\Delta_0(0)$.

Our experimental results for $I(0, 0, 0)$ and α are presented graphically as functions of the value assumed for the parameter ρl. Figure 3 shows that our experimental value of $I(0, 0, 0)$ is in good agreement with the value calculated by using the strong-coupling theory. We have also calculated the London-limit penetration depth λ_L at absolute zero by using Eq. (25), our calculated value for $\xi_0(0)$, and our measured values of $I(0, 0, 0)$.

In order to compare our results with those of other experiments, we carried out calculations of the bulk penetration depth λ at absolute zero, the temperature dependence of the penetration depth near the critical temperature, and the effective penetration depth determined from measurements of the magnetization of thin planar films.

The primary limitations on the accuracy of our results for $I(0, 0, 0)$, $\lambda_L(0)$, and $\lambda(0)$ are due to three types of systematic errors. Each of these makes an extraneous constant contribution to the measured value of $\Delta H_i/\Delta H_0$. The uncertainty is therefore greatest for the thickest film, where we estimate that our results for $I(0, 0, 0)$ and α may be wrong by about 6%. The primary limitation on the accuracy of our result for $d\lambda/dy$ is due to statistical scatter in the data. Our estimates of these errors account for most of the sample-to-sample discrepancies, but it seems likely that variation in the structure of the films is responsible for some additional uncertainty.

We have listed in Table III the most probable values of several parameters. To compute these results we used weighted averages of the values of $I(0, 0, 0)$ and α which we found from our data by assuming $\rho l = 0.7 \times 10^{-15}$ Ωm^2. In finding each average we weighted the value for each sample by the inverse square of the estimated error. The indicated accuracy of each quantity is the standard deviation of the average. We also used the best values of $I(0, 0, 0)$ and α in plotting the experimental curve in Fig. 1.

We conclude that our experimental results for

TABLE III. Best values of parameters.

Parameter	Value
$I(0, 0, 0)/\hbar$	1.37 ± 0.06 sec^{-1}
α	5.51 ± 0.09
$\lambda_L(0)$	315 ± 7 Å
$\lambda(0)$	453 ± 8 Å
$d\lambda/dy$ for $2.75 < y < 6.00$	365 ± 4 Å

$I(0, 0, T)$ agree to within the accuracy of the experiment with the results of the strong-coupling theory. On the other hand, both our theoretical and experimental results are inconsistent with the results of several previous penetration depth measurements. Some of these other measurements are are also inconsistent with each other. However, the comparisons between one type of penetration depth measurement and another depend on surface conditions, a number of theoretical results, and estimates of the parameters ρl and v_F^*. Comparing our data with the one previous penetration depth measurement that is directly comparable, that of Erlbach *et al.* we find close agreement for the normalized kernel $I(0, 0, T)/I(0, 0, 0)$.

ACKNOWLEDGMENTS

We are grateful to J. C. Swihart and to J. P. Carbotte for sending us the computer output on which some of our calculations were based.

---

*Research supported in part by the National Science Foundation under Grants GH-37980 and GH-33634.

†Paper based in part on the Ph. D. thesis of H. R. Kerchner (University of Illinois, 1974) (unpublished).

‡Present address: Oak Ridge National Laboratory, Oak Ridge, Tennessee 37830.

[1]J. Bardeen, L. N. Cooper, and J. R. Schrieffer, Phys. Rev. 108, 1175 (1957).

[2]*Superconductivity*, edited by R. D. Parks (Marcel Dekker, New York, 1969), Chaps. 3, 4, and 11.

[3]L. H. Palmer and M. Tinkham, Phys. Rev. 165, 588 (1968).

[4]R. E. Harris and D. M. Ginsberg, Phys. Rev. 188, 737 (1969).

[5]S. B. Nam, Phys. Rev. 156, 487 (1967); S. B. Nam, (private communication).

[6]W. Shaw and J. C. Swihart, Phys. Rev. Lett. 20, 1000 (1968).

[7]R. F. Gasparovic and W. L. McLean, Phys. Rev. B 2, 2519 (1970).

[8]I. Simon, Phys. Rev. 77, 384 (1950).

[9]J. M. Lock, Proc. R. Soc. Lond. A 208, 391 (1951).

[10]G. E. Peabody and R. Meservey, Phys. Rev. B 6, 2579 (1972).

[11]J. Szymaszek, Acta Phys. Pol. 20, 563 (1961).

[12]M. P. Sarachik, R. L. Garwin, and E. Erlbach, Phys. Rev. Lett. 4, 52 (1960).

[13]E. Erlbach, R. L. Garwin, and M. P. Sarachik, IBM J. Res. Dev. 4, 107 (1960).

[14]D. C. Mattis and J. Bardeen, Phys. Rev. 111, 412 (1958).

[15]H. R. Kerchner and D. M. Ginsberg, Phys. Rev. B 8, 3190 (1973). A more careful examination of the experimental results that were used to obtain $v_F^* = 0.61 \times 10^8$ cm sec^{-1} in Ref. 7 has led us to accept $v_F^* = 0.64 \times 10^8$ cm sec^{-1}. This latter value leads to $\xi_0(0) = 1290$ Å.

[16]A. B. Pippard, Proc. R. Soc. Lond. A 216, 547 (1953).

[17]J. R. Waldram, Adv. Phys. 13, 1 (1964).

[18]D. M. Ginsberg, Phys. Rev. B 7, 146 (1973).

[19]R. G. Chambers, Proc. R. Soc. Lond. A 202, 378 (1950).

[20]K. Fuchs, Proc. Camb. Philos. Soc. 34, 100 (1938).

[21]M. Peter, Phys. Rev. 109, 1857 (1958).

[22]A. V. Bassewitz and G. V. Minnigerode, Z. Phys. 181, 368 (1964).

[23]*Landolt-Börnstein Zahlenwerte und Funktionen aus Physik, Chemie, Astronomie, Geophysik, und Technik* (Springer-Verlag, Berlin, 1959), Vol. 2, Pt. 6, pp. 9, 37.

[24]G. Grimvall, Phys. Kondens. Mater. 8, 202 (1968).

[25]J. R. Anderson and A. V. Gold, Phys. Rev. 139, A 1459 (1965).

[26]R. Stedman, L. Almqvist, G. Nilsson, and G. Raunio, Phys. Rev. 163, 567 (1967).

[27]R. G. Chambers, Proc. R. Soc. Lond. A 215, 481 (1952).

[28]J. E. Aubrey, Philos. Mag. 5, 1001 (1960).

[29]S. B. Nam, Phys. Rev. 156, 470 (1967).

[30]J. C. Swihart (private communication).

[31]P. Vashishta and J. P. Carbotte, Solid State Commun. 8, 161 (1970).

[32]J. R. Schrieffer, D. J. Scalapino, and J. W. Wilkins, Phys. Rev. Lett. 10, 336 (1963).

[33]Ref. 2, Chap. 11.

[34]R. A. Anderson and D. M. Ginsberg, Phys. Rev. B 5, 4421 (1972).

[35]A. H. Silver and J. E. Zimmerman, Phys. Rev. 157, 317 (1967).

[36]H. R. Kerchner, Ph. D. thesis (University of Illinois, 1974) (unpublished).

[37]D. M. Ginsberg and M. J. Melchner, Rev. Sci. Instrum. 41, 122 (1970).

[38]F. B. Hildebrand, *Introduction to Numerical Analysis* (McGraw-Hill, New York, 1956).

[39]B. Mühlschlegel, Z. Phys. 155, 313 (1959).

[40]Ref. 2, Chap. 10.

[41]D. L. Decker, D. E. Mapother, and R. W. Shaw, Phys. Rev. 112, 1888 (1958).

[42]B. J. C. van der Hoeven and P. H. Keesom, Phys. Rev. 137, A103 (1965).

[43]R. H. Bacon, Am. J. Phys. 21, 428 (1953).

[44]J. C. Swihart and W. Shaw, in *Superconductivity*, edited by F. Chilton (North-Holland, Amsterdam, 1971), p. 678.

[45]J. Bardeen (private communication).

[46]R. F. Gasparovic, B. N. Taylor, and R. E. Eck, Solid State Commun. 4, 59 (1966).

[47]R. S. Thompson and A. Baratoff, Phys. Rev. 167, 361 (1968).

[48]A. Baratoff, in *Superconductivity, Proceedings of the Advanced Summer Study Institute, McGill University*, edited by P. R. Wallace (Gordon and Breach, New York, 1969), p. 427.